DTU Library

Ultrafine particle number flux over and in a deciduous forrest

Pryor, S.C.; Barthelmie, R.J.; Larsen, Søren Ejling; Sørensen, L.L.

Ultrafine particle number fluxes over and in a deciduous forest

S. C. Pryor[1] , R. J. Barthelmie[2] , S. E. Larsen[3] , and L. L. Sørensen[4]

[1]Department of Earth and Atmospheric Sciences, Cornell University, Ithaca, New York, USA, [2]Sibley School of Mechanical and Aerospace Engineering, Cornell University, Ithaca, New York, USA, [3]Department of Wind Energy, Technical University of Denmark, Roskilde, Denmark, [4]Arctic Research Centre, Department of Bioscience, Aarhus University, Aarhus C, Denmark

Abstract Ultrafine particles (UFP, particles with diameters (D_p) < 100 nm) play a key role in climate forcing; thus, there is interest in improved understanding of atmosphere-surface exchange of these particles. Long-term flux measurements from a deciduous forest in the Midwestern USA (taken during December 2012 to May 2014) show that although a substantial fraction of the data period indicates upward fluxes of UFP, on average, the forest is a net sink for UFP during both leaf-active and leaf-off periods. The overall mean above-canopy UFP number flux computed from this large data set is -4.90×10^6 m^{-2} s^{-1} which re-emphasizes the importance of these ecosystems to UFP removal from the atmosphere. Although there remain major challenges to accurate estimation of the UFP number flux and in drawing inferences regarding the actual surface exchange from measurements taken above the canopy, the above the canopy mean flux is shown to be downward throughout the day (except at 23.00) with largest-magnitude fluxes during the middle of the day. On average, nearly three quarters of the total UFP capture by this ecosystem occurs at the canopy. This fraction increases to 78% during the leaf-active period, but the over-storey remains dominant over the subcanopy even during the leaf-off period.

1. Introduction and Objectives

Atmosphere-surface exchange of ultrafine particles (UFP, particles with diameters (D_p) < 100 nm) particularly over forests is a major component of aerosol dynamics and therefore plays a key role in determining particle number concentrations and size distributions [*Pryor et al.*, 2008b]. However, significant uncertainties remain regarding the magnitude (and even direction) of the flux and the receptor of, and fate of, particles dry deposited to forest ecosystems (e.g., the partitioning between foliar and nonfoliar elements and/or the canopy versus subcanopy and ground [*Petroff et al.*, 2008]). This has great relevance for developing robust models of particle populations and their associated climate forcing [*Boucher et al.*, 2013] and for understanding the ecosystem response to particles (biogeochemical cycles and potentially the ecosystem health consequences of particle deposition [*Hosker and Lindberg*, 1982]) and the utility of vegetation barriers for UFP removal [*Dadvand et al.*, 2015; *Pataki et al.*, 2011]. Although instrumentation and metrology advancements have greatly improved our ability to measure UFP accurately and at high resolution [*Kumar et al.*, 2016], leading to an increased number of experimental studies of UFP fluxes, relatively few long-term data sets of particle fluxes over forests exist. Additionally, instrument limitations continue to impose major challenges to the application of eddy covariance for flux estimation. Thus, comprehensive understanding of functional dependencies of UFP fluxes remains incomplete, and there is a need for additional observational data for verification and validation of numerical and analytical models of atmosphere-surface exchange. Further, to the authors knowledge only one previous study of simultaneous above and below canopy UFP number fluxes has been undertaken in a coniferous forest [*Grönholm et al.*, 2009]; thus, flux partitioning between the canopy and forest floor is uncertain, and little is known about differences in that partitioning between leaf-on and leaf-off in a deciduous forest.

Key findings from prior research on particle number fluxes in forested environments that provide the motivation for this research include the following:

1. A two-layer eddy covariance system deployed during 14–31 May 2003 at the Station for Measuring Forest Ecosystem-Atmosphere Relations (SMEAR) II measurement station in a Scots pine forest indicated that during downward fluxes under conditions of moderate turbulence (friction velocity (u_*) < 0.25 m s^{-1}) 65% of UFP deposit to the canopy, while under highly turbulent conditions ($u_* > 1.0$ m s^{-1}) the canopy

dominance of the total deposition flux increases to 90% [*Grönholm et al.*, 2009]. Data from this experiment further indicate the median interception fraction by the canopy (leaf area index (*LAI*) of $6 \, m^2 \, m^{-2}$) is 62% (with an interquartile range of 34–74%) [*Grönholm et al.*, 2009].

2. Particle fluxes exhibit large variations with D_p and turbulence regimes, and although forests are known to be an important sink for atmospheric particles, in all previously conducted studies the UFP number fluxes above the canopy are bidirectional [e.g., *Nilsson et al.*, 2001; *Pryor et al.*, 2008a; *Rannik et al.*, 2009]. For example, more than one third of both sub-30 nm and super-30 nm particle number fluxes over a sparse pine forest were found to be upward [*Pryor et al.*, 2013], and in a separate 1 month campaign over a mixed deciduous forest canopy for $D_p = 18$–452 nm, 60% of particle number fluxes were upward [*Gordon et al.*, 2011]. These upward fluxes arise from a range of processes including within canopy storage with subsequent venting from the canopy, entrainment of particle depleted air during destabilization of the nocturnal boundary layer, evaporation of ammonium nitrate particles, anthropogenic particle sources within the flux footprint, growth of particles into the instrument detection range by condensation of water, and/or semivolatile species released within the canopy and flux inaccuracies due to instrument limitations.

3. Particles are not transported as a passive scalar. Rather, there is substantial interplay between coagulation (which reduces the UFP number concentration), condensation (which may grow particles into the detectable range of the instrument), vertical transport, and surface removal [*Pryor et al.*, 2013; *Pryor and Binkowski*, 2004]. A 1-D model applied to 10 days of data from SMEAR II found that "the particle concentration change due to aerosol dynamics frequently exceeded the effect of particle deposition by even an order of magnitude or more" [*Rannik et al.*, 2016].

The purpose of the study reported herein was to develop a long-term data set of particle number fluxes above and below the canopy of a mixed deciduous canopy with which to

1. provide a representative description of UFP number fluxes obtained over an entire year and explore sources of uncertainty in the flux estimates;
2. further explore the causes of upward fluxes in a homogeneous forest environment with very few local sources and a footprint in all directions that is dominated by the forest; and
3. quantify the fraction of total UFP capture that occurs at the canopy of a deciduous forest and evaluate whether it varies significantly temporally or with phenological stage and whether the partitioning between canopy and ground capture of UFP differs from that of a pine forest [*Grönholm et al.*, 2009].

2. Methods

2.1. Site and Instrument Description

The meteorological mast from which data are presented was installed in an expansive secondary successional broadleaved forest (Morgan Monroe State Forest, MMSF, which has an area of >97 km^2) in 1997 (39° 53′N, 86°25′W) [*Schmid et al.*, 2000]. The minimum overforest fetch is 4 km, and thus, the flux footprint at 46 m is entirely dominated by the forest [*Schmid et al.*, 2000]. The flux footprint for subcanopy measurements is naturally considerably smaller than that for the above canopy measurements. Analysis of the SMEAR II site using a Lagrangian footprint model for neutral stratification [*Rannik et al.*, 2003] indicated that the flux footprint for their subcanopy measurements was an order of magnitude smaller than that for the above canopy measurements [*Grönholm et al.*, 2009].

The forest canopy around the tower has recovered from the disruption during tower installation and now encloses the mast (Figure 1). It had a median height of approximately 26–28 m during the sampling period, a seasonal maximum single-sided leaf area index (LAI) of $\approx 4.5 \, m^2 \, m^{-2}$, and is dominated by sugar maple (*Acer saccharum*, 37% of total LAI), tulip poplar (*Liriodendron tulipifera*, 11%), sassafras (*Sassafras albidum*, 4%), and white and black oak (*Quercus alba* and *Quercus velutina*, 6%). A substantial fraction of the total mean LAI (approximately one quarter; Figure 1) is contributed by the understory (associated with a secondary peak in canopy area density at 5 m). The understory is considerably more spatially variable than the forest canopy in terms of both density and height and is dominated by pawpaw (*Asimina triloba*), spicebush (*Lindera benzoin*), and sweet cicely (*Osmorhiza claytonii*) [*Pryor et al.*, 2014]. The aerodynamic roughness length of the site was estimated by using data collected in 1998–1999 as 2.1 ± 1.1 m [*Schmid et al.*, 2000], and the zero-plane displacement height was estimated as 0.75 times the canopy height (h_c) and $0.6 \times h_c$ for the
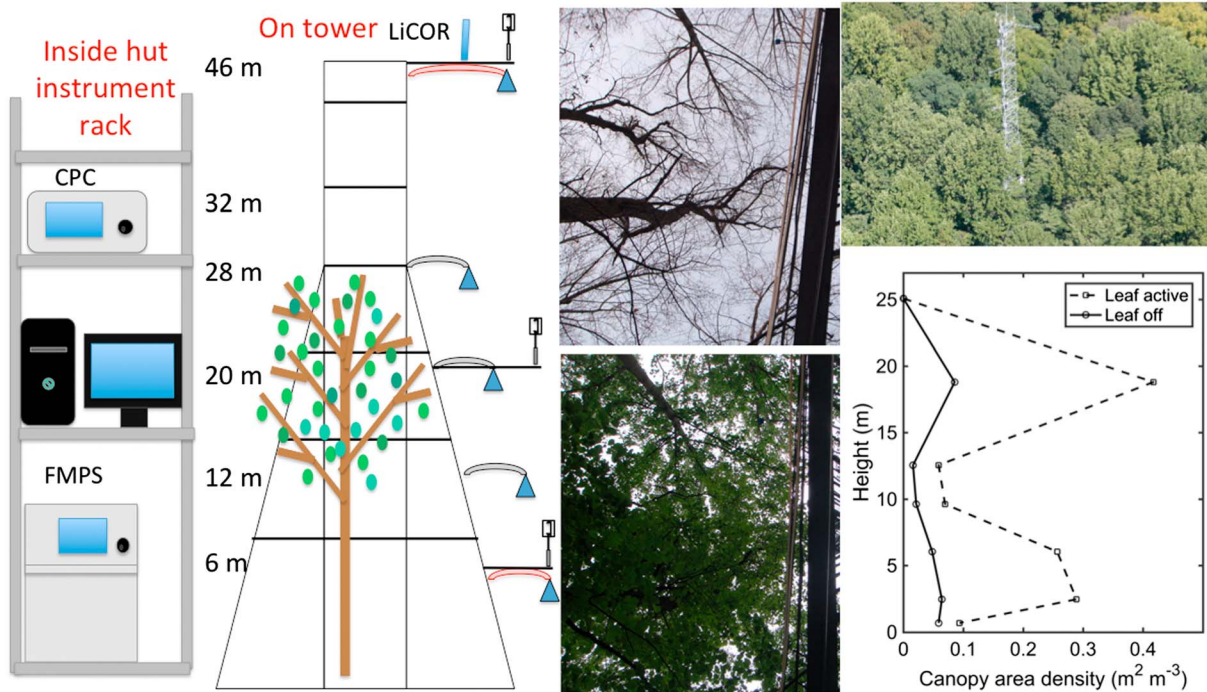
Figure 1. Overview of the sampling design for the particle fluxes at MMSF. The sampling lines shown in grey are used for the 10 min PSD gradients (with measurements with an FMPS and a flow rate of 17 lpm), while the sampling lines shown in red (a flow rate of 25, 27, and 29 lpm) are used for the flux measurements with number concentrations measured at 10 Hz with the CPC 3788. The sonic anemometers were deployed at 46 m, 20 m, and 7 m. There was a 0.5 m vertical offset between the tubing inlet for the flux measurements and the sonic anemometer centerline. Also shown to the right of this schematic are two photographs showing the forest canopy (top) during the minimum LAI and (bottom) at the time of the peak LAI and a photograph taken from an overflight of the site during late August 2013 (top right). The panel in the bottom right shows the profile of the canopy area density ($m^2\,m^{-3}$) as measured on a scaffold tower displaced about 100 m from the flux tower during 2001. The profile from the vegetated season (referred to herein as leaf active) was collected on 1 August 2001, while that for the unvegetated season (leaf off) was acquired on 11 November 2001. The measurements were made at eight heights using a pair of LiCor LAI-2000 instruments [*Froelich et al.*, 2011].

foliated and leaf-off seasons using data from sonic anemometers deployed at 46 m and 34 m in near-neutral conditions (assuming a logarithmic profile) [*Su et al.*, 2004].

Meteorological conditions and atmospheric aerosol particle concentrations exhibit marked seasonality at MMSF (see Figures 2 and 3), so the experimental design of the study reported herein was formulated to permit long-term (one year) measurements of pseudo-simultaneous particle number fluxes in the subcanopy (i.e., below the tree canopy) and above the canopy of a mature deciduous forest. Because the intent was to compare fluxes and deposition velocities above and below the canopy a single particle instrument was employed to prevent spurious results caused by bias in the particle counting efficiency of two instruments. Thus, three Gill WindMaster Pro 3-D sonic anemometers were deployed above (46 m), within (20 m), and below (7 m) the canopy (sampled at 10 Hz), along with copper tubing with inlets at 46 m and 7 m for supply of air to a ultrafine particle condensational counter (TSI CPC3788, a water-based nanoscale condensation particle counter (CPC) that has 50% response for D_p of 2.5 nm, and a risetime of <0.1 s [*Kupc et al.*, 2013]). Using a valve switching system and manifold, air was drawn sequentially down 8.9 mm inner diameter copper tubing from the 46 m (30 min past the hour to the top of the hour) and 7 m sampling levels (0 to 30 min past the hour) and subsequently sampled by the CPC (with data reported at 10 Hz). The instrument exhaust flow was returned to the manifold to avoid a large pressure drop across the instrument. Copper tubing was selected for this application because its malleability enables use of very smooth bends and very few joins. Abrupt pressure changes within the manifold caused significant disruption of the CPC internal flow resulting in multiple instrument faults. Thus, when switching between the two sampling heights the flow along a given sampling line was gradually reduced to zero, the flow controllers activated to switch to the other sampling line and then the flow rate was increased to the full volumetric flow rate, with this entire procedure occurring over 120 s. To avoid unstable flow during the valve switching, we use only the central 24 min in each 30 min period to derive an estimate of the particle number flux at each level. This decision
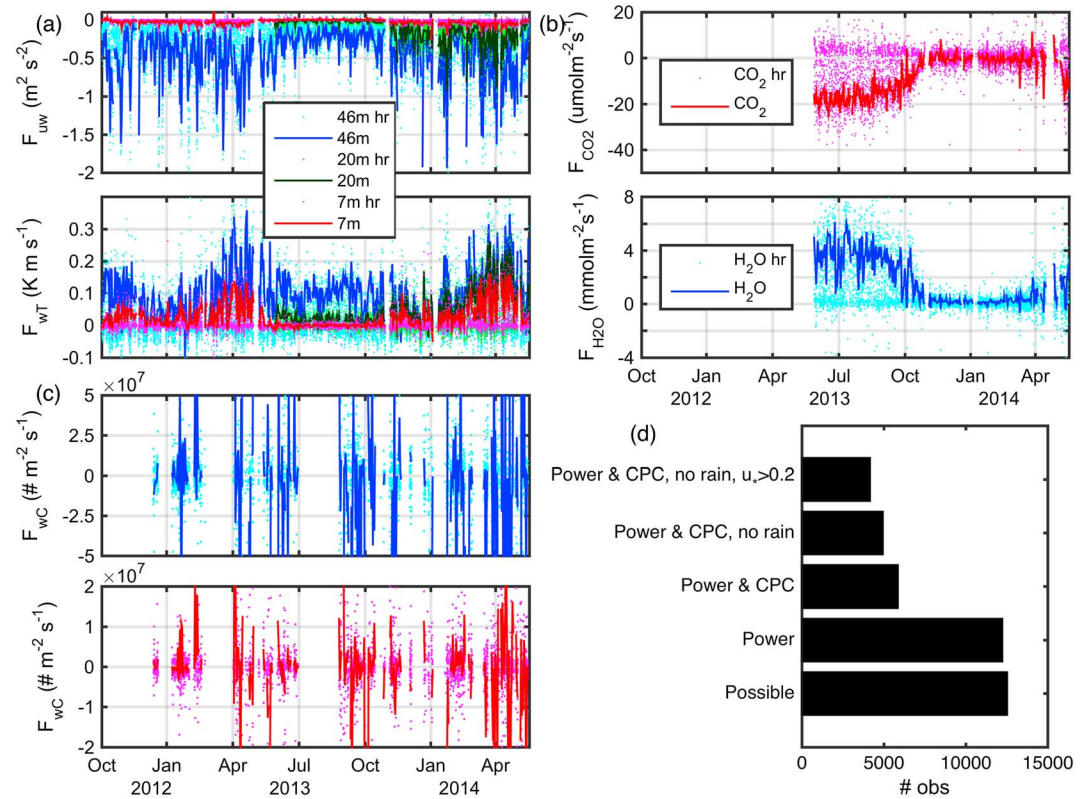
Figure 2. Fluxes of (a) momentum (F_{uw}) and sensible heat (F_{wT}) from the three Gill Windmaster Pro sonic anemometers at 46 m, 20 m, and 7 m; (b) carbon dioxide (F_{CO2}) and H_2O (F_{H2O}) from the LiCOR LI-7200 and Gill Windmaster Pro sonic anemometer at 46 m; and (c) particle number (F_{wC}) from the Gill Windmaster Pro sonic anemometers at 46 m and 7 m and the CPC3788. Also shown in Figures 2a–2c are solid lines which denote the midday average fluxes (computed as the mean flux value from each calendar day of values during 10:00–14:00, inclusive). Figure 2d shows the number of hours on which data collection was possible (possible) and those available when a screen is applied for power outages at the site, for CPC faults, for the occurrence of rain and for u_* at 46 m > 0.2 m s^{-1}.

regarding the sampling time at each level was a compromise between the desire to increase the sample number in each flux estimate while also retaining a high probability that the fluxes above and below the canopy were sampled within a reasonable period of time for stationarity to be assumed.

It should be noted that in the 6 week the dual-level deployment at SMEAR II to examine above and below canopy fluxes, the subcanopy measurements were taken at 2 m above ground level, while in the long-term deployment at MMSF we selected a height of 7 m due to the presence of a significant subcanopy vegetation layer centered at about 5 m (Figure 1). Further, while the two-level EC data set from SMEAR II was collected during a period with continuous snow cover, snow is only intermittently observed at MMSF. During the two winters (December 2012 to February 2013 and December 2013 to February 2014) for which the UFP number fluxes were computed, nonzero snow depth was reported less than half of days at the closest first-order National Weather Station (NWS) 45 km to the north of MMSF (in Indianapolis, IN) and fewer than 20% of days had nonzero snow depth at the next closest first-order NWS station 120 km to the south (Louisville, KY). A final important difference between the research reported herein and that conducted at SMEAR II pertains to the difference in instrumentation. The sonic anemometers (Gill Solent 1012R and Gill WindMaster Pro) are comparable, but the CPC used at SMEAR II is a TSI model 3010 which has a 50% detection limit at a $D_p = 10$ nm, while the CPC 3788 has a 50% detection limit at 2.5 nm.

There is increased uncertainty in flux estimates derived in low-turbulence environments [*Teklemariam et al.*, 2009], and a range of different approaches have been taken within the particle flux community with regards to application of a threshold friction velocity (u_*) for screening out highly uncertain fluxes. For example, while *Grönholm et al.* [2009]] did not apply a u_* threshold, *Buzorius et al.* [2001], *Gordon et al.* [2011], and *Pryor et al.* [2008a] excluded fluxes obtained under conditions with u_* less than 0.2 m s^{-1} and *Rannik et al.* [2009] applied
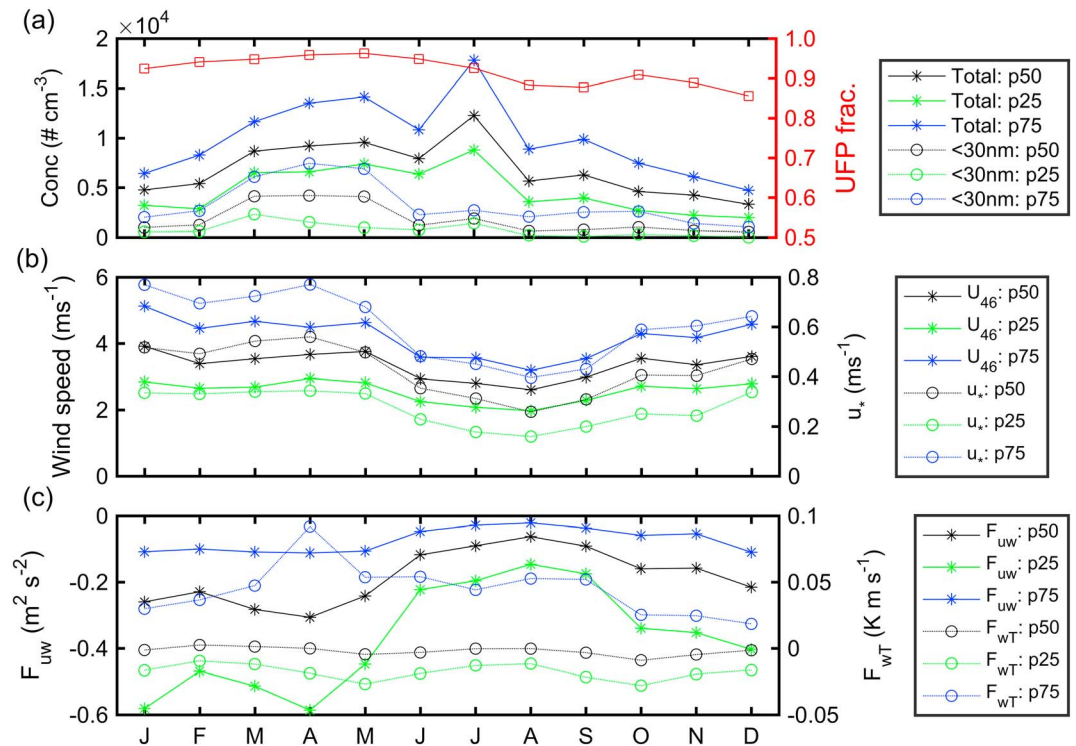
Figure 3. Précis (median (p50) and interquartile range (p25 and p75)) of (a) particle concentrations (i.e., total number conc. D_p: 6–500 nm, and for D_p 6–30 nm) as measured at 28 m (just above the forest canopy) using an FMPS by calendar month, along with the median and interquartile range of (b) wind speed (U_{46}) and friction velocity (u_*), (c) momentum (F_{uw}) and heat flux (F_{wT}) at 46 m. Also shown in Figure 3a (right axis) is the mean fraction of the total particle number concentration (D_p: 6–500 nm) in the FMPS measurements at 28 m that were associated with $D_p < 100$ nm (shown in red and labelled UFP frac.).

a threshold of $0.1\,\mathrm{m\,s^{-1}}$. Here we exclude fluxes using a u_* threshold of $0.2\,\mathrm{m\,s^{-1}}$, but acknowledge this will tend to lead to under-represent summertime conditions, due to the lower wind speeds and u_* at the site particularly during August (see Figure 3).

During the second half of the measurement period a LiCOR LI-7200 (sampled at 10 Hz) was also deployed at 46 m to obtain simultaneous measurements of fluxes of water vapor (H_2O) and carbon dioxide (CO_2) using output from the same sonic anemometer used for the particle number fluxes. The resulting data are used in the scalar similarity analysis and in determining the timing of leaf-senescence. Herein we assume that the canopy is fully active (referred to herein as "leaf-active") from the first date on which the 5 day running mean of the net CO_2 flux at midday (10:00–14:00, inclusive) $< -10\,\mu\mathrm{mol\,m^{-2}\,s^{-1}}$ and the canopy ceases to be fully active in the fall on the first date where the 5 day running mean of the net CO_2 flux at midday (10:00–14:00, inclusive) $> -10\,\mu\mathrm{mol\,m^{-2}\,s^{-1}}$ (see example CO_2 fluxes in Figure 2b). The leaf-off period (referred to herein as "leaf-off") is defined as the period from the first day in fall when the 5 day running mean of the net CO_2 flux at midday $>0\,\mu\mathrm{mol\,m^{-2}\,s^{-1}}$ and concludes in the spring on the first day when the 5 day running mean of the net CO_2 flux at midday $< 0\,\mu\mathrm{mol\,m^{-2}\,s^{-1}}$. As an example, in 2013 the leaf-active period defined this way begins on 22 April and ends on 26 September, and the leaf-off period begins on 28 October 2013 and ends on 2 April 2014. Prior to deployment of the LI-7200, the CO_2 fluxes used for determining leaf-active versus leaf-off periods derive from AmeriFlux reported values obtained by using a CSAT-3 located at 46 m and air drawn down Teflon tubing to a closed-path LiCOR LI-7000 located in the temperature controlled instrument hut (with the CPC) at the bottom of the tower [*Roman et al.*, 2015]. When conditionally sampled to exclude precipitation and $u_* < 0.2\,\mathrm{m\,s^{-1}}$, hourly mean CO_2 fluxes computed by using data from the LiCOR LI-7200 and Gill sonic and those from the LiCOR LI-7000 and CSAT-3 exhibit a least squares regression fit with a slope of 1.004, an intercept of -0.128 and an adjusted r^2 of 0.986 ($n = 5183$), indicating good closure for flux measurements from the two systems.
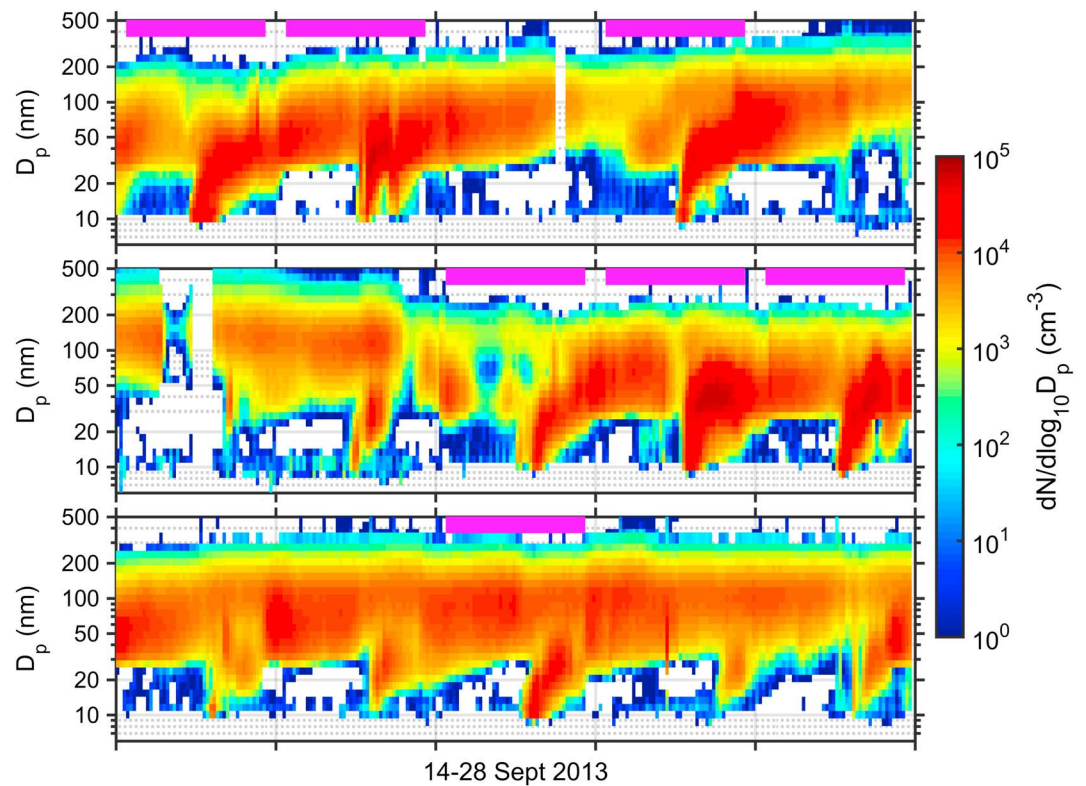
Figure 4. Example particle size distribution (PSD) at 28 m from the FMPS operated on the gradient sampling system over a 15 day period during 14–28 September 2013 (see details of the gradient sampling system given in *Pryor et al.* [2014]). Also shown (by the magenta blocks) are days that are identified as clear nucleation events by the automated protocol presented in *Sullivan and Pryor* [2016]. This event classification was used to identify class-A type nucleation events that are used herein to examine UFP number fluxes during new particle formation.

As mentioned above, the aerosol particle population exhibits marked variations over the course of the year, with highest number concentrations during the summer months but a greater prevalence of sub-30 nm diameter particles during the spring (Figure 3a). The UFP (i.e., $D_p < 100$ nm) contributed an average of 92% of particles in the diameter size range of 6–500 nm as measured by an Fast Mobility Particle Sizer (FMPS) deployed to sample the size distribution at 28 m (i.e., close to the canopy). New particle formation (NPF) is frequently observed at MMSF particularly during spring [*Pryor et al.*, 2014]. Given the postulated importance of particle nucleation to both the total number concentration of UFP and vertical fluxes of particles [*Pryor et al.*, 2013; *Rannik et al.*, 2009], here we also conditionally sample the fluxes based on an automated nucleation detection scheme. This scheme is designed to identify unambiguous A-class NPF events in which the occurrence of large quantities of nucleation mode particles is followed by sustained growth [*Dal Maso et al.*, 2005]. In brief, a NPF event is identified on a given calendar date if the minimum nucleation mode geometric mean diameter (i.e., the GMD for $D_p < 30$ nm, D_{gNuc}) occurs within 10 h of the peak nucleation mode number concentration and the difference in the geometric mean diameter for $D_p < 100$ nm and D_{gNuc} is less than 10 nm, and both new particle formation rates and growth rates can be reasonably calculated (e.g., the variance explanation of a regression fit for nucleation mode geometric mean diameter to time used to compute the growth rate (over a 3 h period) is ≥0.5) [*Sullivan and Pryor*, 2016]. The occurrence of nucleation is identified by using this scheme applied to particle size distributions sampled at 28 m with a TSI Fast Mobility Particle Sizer (FMPS 3091, in 32 logarithmically spaced channels in D_p 6–520 nm) attached to a gradient sampling system in which particle size distributions (PSDs) were sequentially sampled at 28, 20, and 12 m [*Pryor et al.*, 2014] (see examples shown in Figure 4). Consistent with previous subjective NPF analyses based on measured PSD at MMSF [*Pryor et al.*, 2014; *Pryor et al.*, 2010], the automated scheme indicates a clear seasonality in nucleation occurrence with highest frequency in spring and a secondary maximum in fall. Forty four of the unambiguous A-type NPF events for which simultaneous UFP number fluxes are available were selected for inclusion in the analyses presented herein.

While the LiCOR and sonic anemometers operated without significant problems except during power failures at the site (Figures 2a and 2b), the deployment of the CPC was subject to a range of technical issues primarily related to pressure fluctuations when switching between the sampling lines. Initially, the flow rate in the copper tubing was maintained at 25 lpm, but visual inspection of the power spectra of UFP number concentrations led to concerns regarding whether the flow is fully turbulent at that flow rate. Hence, the flow rate was subsequently increased to 27 lpm and then to 29 lpm (equating to mean Reynolds numbers (Re, averaged over a range of observed air temperature and thus variations in the kinematic viscosity of air) of 4096, 4424, and 4752, respectively). The engineering lag times for the three flow rates for transfer through the tubing are 8.9, 8.3, and 7.7 s and were used herein combined with a windowing approach centered on these lag times to determine the timing and magnitude of the maximum absolute value of the covariance (following *Aubinet et al.* [2000]). Although UFP number fluxes from the entire measurement period (December 2012 to May 2014) are reported herein, an analysis is also undertaken to compare fluxes from October 2013 to May 2014, when a consistent flow rate of 29 lpm was employed. Even after the flow rate and switching difficulties were resolved, the CPC experienced several faults including those related to flooding of the instrument due to failure of the liquid drain valve and blockage of the airflow due to clogging of the internal tubing and critical orifice. Thus, although the UFP number flux estimates were collected over a period spanning from December 2012 to May 2014, these technical problems caused a substantial amount of data loss, and hence, the particle number flux data set is highly fractured (Figures 2c and 2d). Additional data screening to exclude periods when precipitation was reported by a Texas Electronics TE525 tipping bucket rain gauge deployed at 46 m, or when $u_* < 0.2 \, \mathrm{m \, s^{-1}}$ further reduced the sample size (Figure 2d). Nevertheless, since the instrument faults were not related to specific meteorological conditions, the resulting UFP number flux data set is assumed to be reasonably representative, although it is biased toward sampling conditions wherein the canopy was inactive relative to a typical calendar year. For example, using the definitions of leaf-active and leaf-off described above, there are almost equal numbers of days in each class (the ratio of the number of hours; leaf-active/leaf-off is 1.01), while the 4931 h on which fluxes above and below the canopy were computed indicates a bias toward sampling leaf-off conditions (the ratio leaf-active/leaf-off is 0.82). In all analyses presented herein the fluxes were conditionally sampled to exclude periods when u_* at 46 m was below $0.2 \, \mathrm{m \, s^{-1}}$. This slightly enhances the bias toward the representation of leaf-off conditions and results in a sample size of hours with simultaneous particle number fluxes above and below the canopy of 4147 h.

2.2. Flux Analysis Methodology

As described above, we seek to generate representative estimates of the probability distribution of UFP number fluxes, quantify the uncertainties associated with those fluxes and their magnitude relative to other terms in the continuity equation, and advance understanding of both the causes of upward fluxes and the partitioning of the UFP flux between the canopy and ground. In this section we describe the methodologies employed in these analyses. We start with a brief discussion of our application of eddy covariance for flux estimation (section 2.1), followed by the approaches used to assess the robustness of the fluxes (section 2.2.2), and quantify the storage flux (section 2.2.3). In section 2.2.2 we introduce use of scalar correlation coefficients to examine causes of upward fluxes and end this methodological description with metrics used to assess the partitioning of the deposition flux between the canopy and ground (section 2.2.5).

2.2.1. Flux Estimation by Eddy Covariance

Time series of 10 Hz data from the sonic anemometers were subject to a 3-D coordinate rotation using planar fitting to align the u component with the mean wind direction and to result in zero mean vertical velocity (w). Then vertical fluxes of particle numbers (F) were calculated for all periods when no fault or warning message was reported by the CPC, by first removing outliers from the particle number concentrations (C) (defined as particle number concentrations beyond 5 standard deviations from the mean value during that half-hour period), and then applying flux estimation using the eddy covariance (EC) approach:

$$F = \overline{w'C'} \tag{1}$$

where C' and w' are deviations from the time averaged values.

Since one of our research objectives is to compare with particle flux estimates from the SMEAR II research station [*Grönholm et al.*, 2009; *Rannik et al.*, 2009], as in that prior research we do not apply either the

Webb correction or the correction for saturation ratio fluctuations. The Webb correction is applied to correct for the influence of water vapor fluxes on the content of the parameter of interest relative to the total moist air [*Webb et al.*, 1980], and thus is appropriate for use in estimating UFP number fluxes. However, it is likely of comparatively small magnitude, and thus, exclusion of this correction will likely have a very modest impact on the UFP number fluxes reported herein. For example, *Gordon et al.* [2011] found that the Webb correction did not exceed 1% of the flux for any of the 328 sample periods and *Pryor et al.* [2008c] found that the mean Webb correction over 1377 30 min periods was <1%. The correction for the influence of deliquescence is potentially larger. These correlated fluctuations between the ambient water vapor saturation ratio and w (evident in the dominance of upwards fluxes of water vapor shown in Figure 3c) will tend to systematically increase the likelihood of upward particle number fluxes since in the presence of vertical gradients of humidity, higher humidity, at/near the canopy will tend to grow small particles into the detectable size range of the CPC. For example, *Pryor et al.* [2008c] estimated it to be almost one third of the absolute UFP flux magnitude in a 5 week data set, using the approach of *Kowalski* [2001] and the following assumptions: the particle ensemble is moderately hygroscopic and the PSD conforms to a Junge distribution. In a separate data set, and using slightly different assumptions, *Gordon et al.* [2011] found that the mean correction to F was 26%. However, correct quantification of this effect for UFP is very challenging and is partly dependent on assumptions regarding the PSD and drying of the particles within the sampling lines and instruments [*Rannik et al.*, 2009]. Since we employ long sampling lines and one of the objectives is to compare the canopy-ground flux partitioning to the study at SMEAR II that do not apply Webb or saturation ratio corrections, the F estimates reported herein have also not been subject to these corrections.

2.2.2. Uncertainties

The uncertainty on the fluxes of two scalars (w and x) ($\overline{w'x'}$) is approximated using [*Wyngaard*, 1973]

$$\partial F^2 = \frac{2\tau}{T} \times \left(\overline{(w'x')^2} - \overline{w'x'}^2 \right) \tag{2}$$

where δF is the uncertainty, T is the time interval used to compute F, and τ is assumed to be approximately the effective measurement height ($z = z_r - d$, where z_r is the measurement height and d is the displacement height $= 3/4 h_c$, where $h_c =$ canopy height [*Kaimal and Finnigan*, 1994]) divided by the mean horizontal wind speed (U) and is corrected for the positive bias using the Monin-Obhukov length (L) (by a factor of 2 and 6, for neutral and unstable conditions and stable conditions, respectively [*Rannik et al.*, 2009]).

Power spectra of vertical wind speed (w) and sonic virtual temperature (T) from both heights (7 m and 46 m) conform relatively closely to the expected $-2/3$ slope of the inertial subrange (Figure 5), although as in prior research the power spectrum of w in the subcanopy generally exhibits a lower slope than $-2/3$ [*Kaimal and Finnigan*, 1994], due to the presence of canopy-induced wakes [*Finnigan*, 2000]. The particle number concentration spectra from both heights do not exhibit such close accord with classical forms and frequently show both the absence of a clearly resolved peak at low frequencies particularly at the 7 m sampling level (possibly due to the short time period used; 24 min or the inclusion of periods when the particle concentration was nonstationary), evidence of aliasing, and white noise at high frequencies (characterized by a slope of +1 [*Eugster and Senn*, 1995]) (see examples in Figure 5). Thus, the total particle number flux as derived using eddy covariance may underestimate the true flux due to the absence of the contribution from some scales (specifically the high frequency area). To address this issue, UFP number fluxes from the 46 m measurement are also estimated by using an off-line (postprocessing) relaxed eddy accumulation (REA) approach [*Held et al.*, 2008; *Pryor et al.*, 2008c]. Although application of REA requires scalar similarity and does not negate all of the challenges in estimating particle number fluxes, the potential advantage of the postprocessing REA approach is that the flux is derived from a difference in mean concentrations and thus maybe less sensitive to a loss of information at high frequencies. F_{REA} is computed from

$$F_{REA} = \beta \times \sigma_w \times \left(C_{up} - C_{down} \right) \tag{3}$$

where β is a proportionality factor (the Businger coefficient) that can be experimentally determined from the sensible heat flux, the dead-bandwidth (here $0.5\sigma_w$), and sampling height. C_{up} and C_{down} are average concentrations from samples collected when w is positive and negative, respectively (and exceed the dead-band value), and σ_w is the standard deviation of w. For an ideal Gaussian joint probability distribution of the vertical wind speed and the scalar concentration, β has a well-defined value of 0.627 [*Wyngaard and Moeng*, 1992]. Transport from organized motion alone gives a theoretical factor $\beta = 0.54$ [*Katul et al.*, 1996]. However,
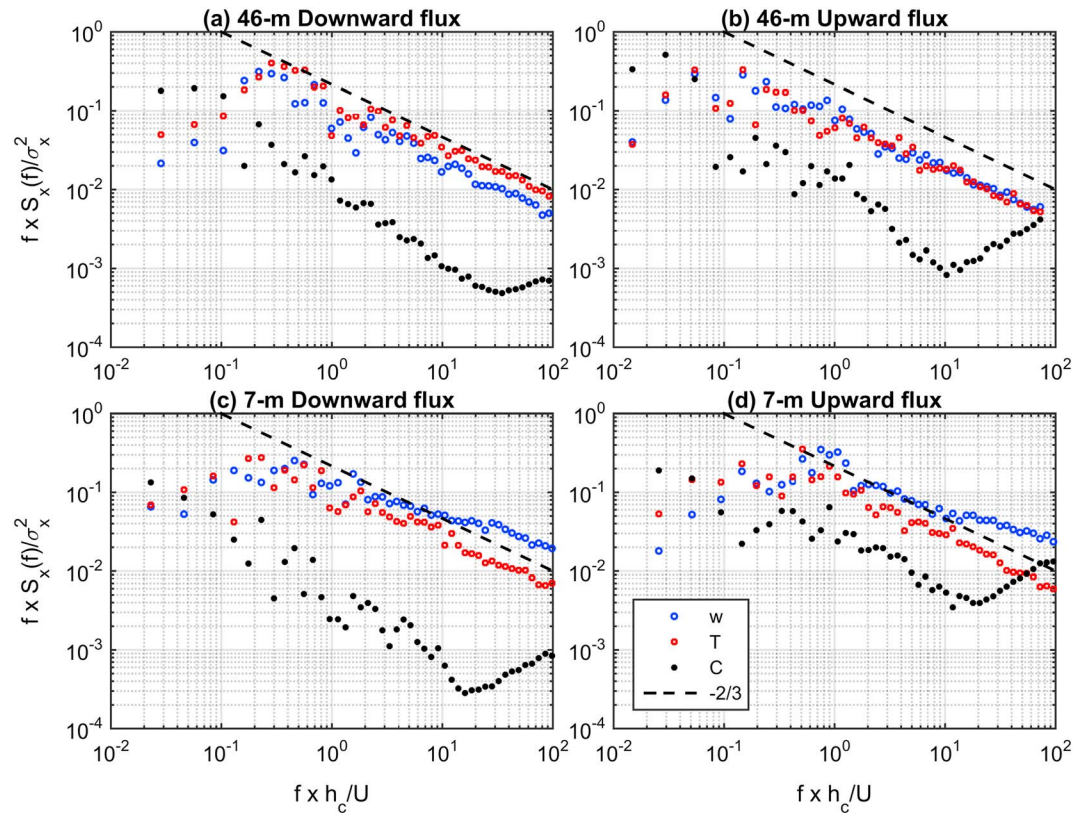
Figure 5. Example power spectra of the vertical wind speed (w), sonic virtual temperature (T), and particle number concentration (C) computed from data collected (a and b) above the canopy (46 m) and (c and d) below the canopy (7 m) for four example half-hour periods during downward particle number fluxes (Figures 5a and 5c) and upward particle number fluxes (Figures 5b and 5d). These cases were selected to exhibit similar friction velocity ($u*$) and Monin-Obhukov length (L) at 46 m. The values of z/L are -0.43 (Figure 5a), -0.48 (Figure 5b), -0.33 (Figure 5c), -1.1 (Figure 5d), and $u*$ is 0.53 m s^{-1} (Figure 5a), 0.62 m s^{-1} (Figure 5b), 0.60 m s^{-1} (Figure 5c), and 0.50 m s^{-1} (Figure 5d), where z for the above canopy is z-d (where d is the displacement height, $3/4 \times h_c$, where h_c is the canopy height), and for below canopy $z = 7$ m. In this figure f denotes frequency, h_c is the canopy height (28 m), U is the mean horizontal wind speed, and σ_x^2 is the variance of the parameter x (w, T or C) under consideration. Also shown in each panel is a dashed line with a slope equal to $-2/3$.

experimentally determined β coefficients for fluxes of heat, moisture, and CO$_2$ typically range from 0.51 to 0.62 [*Katul et al.*, 1996]. Mean beta (β) computed in this study from the measured heat flux is 0.40 (standard deviation (σ) = 0.08) which is consistent with previously reported experimental data collected by using a dead-band threshold w of $0.5\sigma_w$ [*Businger and Oncley*, 1990]. Comparing UFP number fluxes from EC and REA is in reality an indirect way to compare the similarity between cospectra of heat fluxes (T-w) and particle fluxes (C-w). If the UFP number fluxes estimated from EC and REA exhibit a high degree of agreement it is likely that the C-w and T-w cospectra exhibit similar distributional forms.

2.2.3. Storage Flux

The height and density of the forest canopy in MMSF are relatively homogenous in the horizontal and the topography is relatively simple; thus, we assume horizontal homogeneity, steady state conditions, and neglect the sedimentation term for UFP in the continuity equation. Given these simplifying assumptions, integration over z from 0 to the measurement height (z_r) gives the following:

$$\int_0^{z_r} \frac{\partial C}{\partial t} dz + \overline{w'C'}(z_r) = \int_0^{z_r} \overline{S}\, dz \tag{4}$$

That is, the storage flux term (i.e., the rate change of concentration below z_r) plus the flux derived from eddy covariance at z_r are balanced by the net sum of sources and sinks below z_r per unit area. Here we estimate the storage flux (F_{Store}) [*Rannik et al.*, 2009] for the above canopy fluxes from

$$F_{Store} = z\, \frac{C(\text{end}) - C(\text{start})}{T} \tag{5}$$

where C(text) is the mean particle number concentration in the first 120 s (start) and the last 120 s (end) of the 24 min period ($T = 24 \times 60$ s) and z is the effective sampling height. Positive values for F_{store} indicate an increase in particle concentrations either due to particle formation and/or venting of particles up from below the measurement level (e.g., possibly as a result of storage within the canopy). Conversely, negative F_{store} implies a decrease in concentrations consistent with either deposition and/or entrainment of particle depleted air from aloft and/or loss of particles due to coagulation.

2.2.4. Diagnosing Upward Fluxes

In the absence of local UFP sources, entrainment of relatively particle-depleted air from above the nocturnal inversion layer and venting of particles from the canopy have been invoked as the primary possible causes of upward fluxes of UFP. We explore these processes by using correlation coefficients between scalar fluctuations (R_{xy}) [*Pryor et al.*, 2008a]:

$$R_{xy} = \frac{\overline{x'y'}}{\sigma_x \sigma_y} \tag{6}$$

Our a priori expectation was that during the day, in the absence of particle uptake/release of water vapor, R_{qT} and R_{wT} will largely be positive reflecting loss of sensible and latent heat from the canopy. Conversely, during the early nighttime hours R_{qT} will typically tend to be negative as the canopy loses sensible heat but water vapor is deposited thereto. During the early morning R_{wT} may become negative during entrainment of warmer air from above the nocturnal inversion. We examine the probability distributions of R_{CT}, R_{wT}, and R_{qT} at 46 m during periods of upward particle fluxes to infer whether the positive particle fluxes derive mainly from local surface-driven turbulence (e.g., updrafts of air carrying particle-enriched air away from the canopy) or entrainment of air from above the inversion (e.g., downdrafts of air carrying particle depleted air down toward the canopy). In order to maximize the signal-to-noise ratio we focus this analysis on the upper 25th percentile of particle fluxes (i.e., the largest magnitude upward fluxes).

2.2.5. Flux Partitioning Between the Canopy and Ground

Following *Grönholm et al.* [2009], to examine the partitioning of the dry deposition of particle number between the forest canopy and forest floor we select only downward fluxes and compute both the flux ratio (FR) between fluxes at 7 m and 46 m (i.e., F_7/F_{46}) and the interception fraction (I) from the ratio of below to above canopy deposition velocities using [*Ould-Dada*, 2002]

$$I = 1 \frac{v_{ds}}{v_d} \tag{7}$$

where the deposition velocities above and below the canopy (v_d and v_{ds}, respectively) were computed as the ratio of F_z/C_z, where F is the particle number flux and C is the mean concentration at that height (z, 46 m or 7 m).

Leaf surface microroughness is speculated to play a key role in determining leaf capture of UFP, and there is evidence that deliquescent particles may be taken up by both the cuticle and through the stomata [*Burkhardt*, 2010]. To examine whether it is possible to differentiate the uptake by active leaves (versus senescent leaves and/or woody materials in the canopy) we also compute I for periods when the midday CO_2 flux was down and when the midday CO_2 flux was upward. We further examine whether the effect of stomata penetration can be detected by comparing FR within the leaf-active dates during the daytime (i.e., 10:00–16:00, inclusive) and during the nighttime (i.e., 22:00–04:00, inclusive).

3. Results

3.1. Particle Fluxes

3.1.1. Flux Climatology

Particle number fluxes above the canopy (at 46 m) were downward 54 and 56% of the time, during the whole experiment (i.e., at all three flow rates) and when the sampling flow rate was 29 lpm, respectively (Figure 6a). For measurements at 7 m, half of the fluxes were downward under all sampling flow rates. Based on this analysis, the *Re* associated with flow rates of 25, 27, and 29 lpm, and inspection of the C power spectra it appears that the fluxes from the entire measurement period (i.e., under each of the sample flow rates) can be used with equal validity.

The pearson correlation coefficient (r) of the entire data set of flux estimates from EC and REA is 0.95 (Figure 6 d), and the mean bias in the EC estimates of F at 46 m is -2% relative to that from REA, consistent with the expectation that the inability of the measurement system to capture all the scales that contribute to the flux
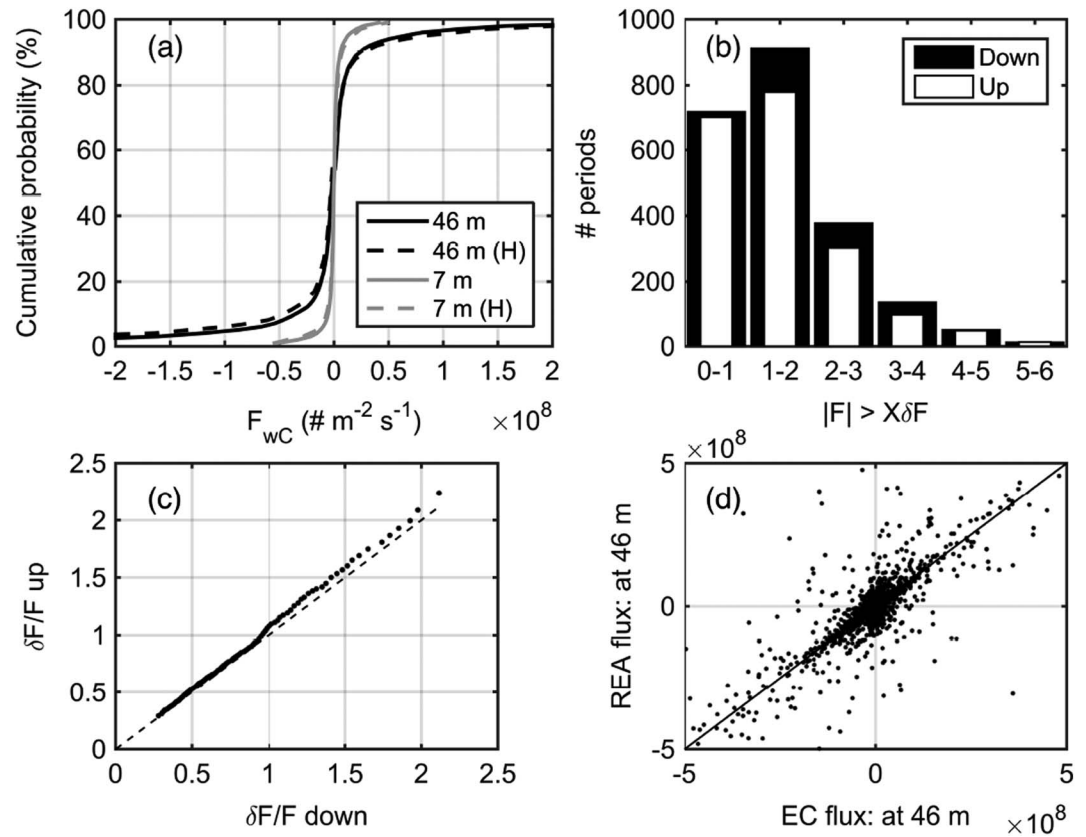
Figure 6. (a) Cumulative density function of particle number flux (F_{wC}) at 46 m computed using EC (total no. of hours with valid total number particle fluxes and $u_* > 0.2\ \mathrm{m\ s^{-1}}$ at 46 m, $n = 4152$). The grey lines denote the cumulative density function computed from all data periods where $u_* > 0.2\ \mathrm{m\ s^{-1}}$, while the black lines are computed solely for the period when the flow rate in the sampling line was 29 lpm (denoted by 'H' in the legend). To aid legibility the x axis is truncated the absolute range of fluxes at 46 m extends from -6.5×10^9 to $2.2 \times 10^9\ \mathrm{m^{-2}\ s^{-1}}$, while the fluxes at 7 m range from -2.2×10^8 to $2.6 \times 10^8\ \mathrm{m^{-2}\ s^{-1}}$. (b) Bar chart of the number of periods with particle number fluxes (F) at 46 m in excess of X times the uncertainty on the flux (δF) conditionally sampled by the direction of the flux. (c) Empirical quantile quantile plot of the relative flux uncertainty ($\delta F/F$) in upward and downward flux periods. Values are shown for the 5th to 95th percentiles, along with a 1:1 line. (d) Scatterplot of particle number flux at 46 m (in # $\mathrm{m^{-2}\ s^{-1}}$) as derived using eddy covariance and REA. Also shown in Figure 6d is a 1:1 line.

leads to a small negative bias. While all of the assumptions implicit in flux estimation by EC are not fully met, the agreement between fluxes estimated by REA and EC implies that the flux estimates provided herein can be viewed with some degree of confidence.

The fluxes at 46 m exceeded the uncertainties on them (δF) in 68% of the periods with downward fluxes, and 64% of upward flux cases, and exceed $2\delta F$ in 26% of downward flux cases and 24% of upward flux cases (Figure 6b). Consistent with analyses of a long-term data set from SMEAR II [*Rannik et al.*, 2009], the relative flux uncertainties ($\delta F/F$) indicate slightly larger values for the mean, median, and upper-percentiles during upward fluxes (Figure 6c). However, a Wilcoxon signed rank test applied to test whether $\delta F/F$ differs during upward and downward flux periods fails to reject the null hypothesis of a median value of 0 at a significance level of 5%. Thus, the average relative magnitude of the uncertainties associated with upward fluxes does not appear to be statistically larger than that associated with downward fluxes. While it is tempting to report only fluxes during periods when $F > X\delta F$ (where X is a multiplier on the uncertainty), in the absence of a physical justification for doing so, and because this may bias the resulting flux statistics, in developing the estimates of climatologically representative fluxes we equally weight all flux estimates.

The ensemble average UFP number flux at 46 m computed as the mean of all F values is $-4.9 \times 10^6\ \mathrm{m^{-2}\ s^{-1}}$, while the median value is $-1.7 \times 10^6\ \mathrm{m^{-2}\ s^{-1}}$ (interquartile range (IQR): -6.5 to $5.3 \times 10^6\ \mathrm{m^{-2}\ s^{-1}}$) Comparable values of the mean and median for below the canopy are $-1.1 \times 10^6\ \mathrm{m^{-2}\ s^{-1}}$ and
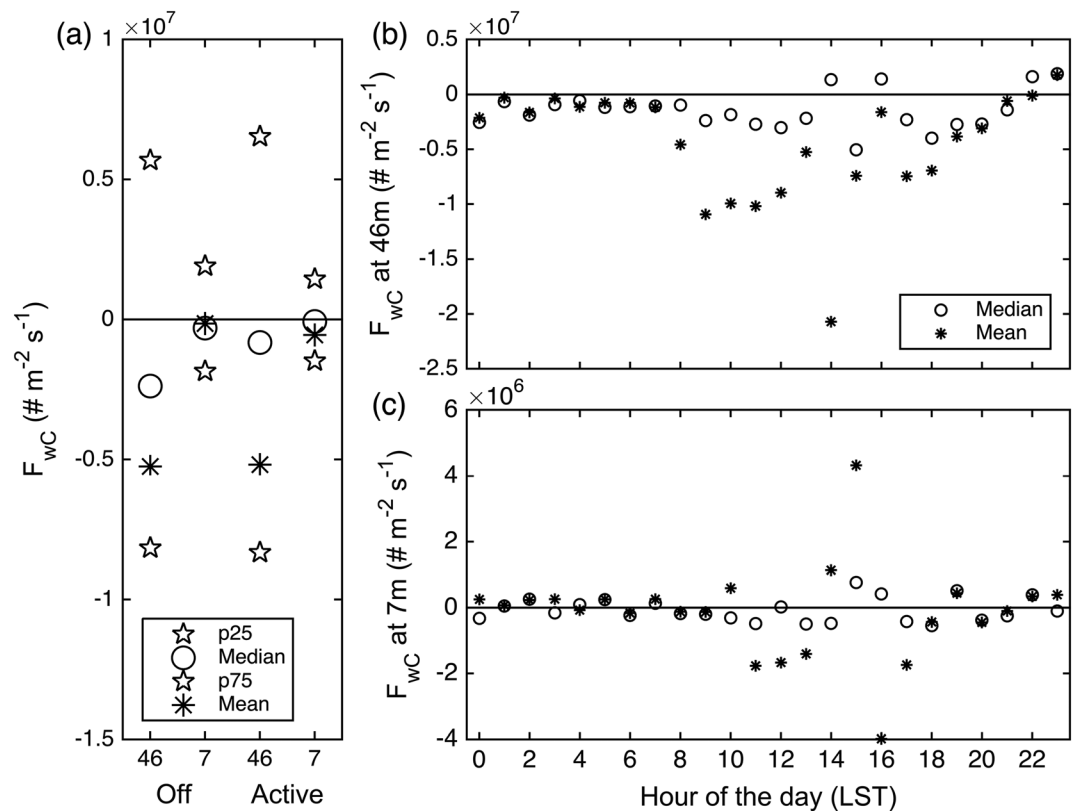
Figure 7. (a) Median, mean, and interquartile range (p25 and p75) of EC-derived UFP number fluxes (F_{wC}) at 46 m and 7 m heights during the leaf-off and leaf-active periods of the year. (b and c) Mean and median diurnal cycles of EC-derived particle number fluxes at the two sampling heights 46 m (Figure 7b) and 7 m (Figure 7c) for all data periods.

$-1.3 \times 10^5 \, \text{m}^{-2} \, \text{s}^{-1}$, respectively (IQR: -1.7 to $1.7 \times 10^6 \, \text{m}^{-2} \, \text{s}^{-1}$). The median flux at both levels is downward (negative) during both the leaf-off and leaf-active seasons, but the flux values above the canopy exhibit considerably more variability during the leaf-active season as manifest in the larger interquartile range (Figure 7a). The diurnal cycle of fluxes above the canopy is such that in all hours except 23:00 local standard time (LST) the mean flux is downward, but the mean flux magnitude is, consistent with a priori expectations, larger during the middle of the day (Figure 7b). During two of the afternoon hours (e.g., at 16:00 LST) the mean and median values are of opposite sign again, indicating the large variability in flux magnitude and direction during this part of the day. Below the canopy the fluxes are of smaller magnitude and the diurnal variability is greatly suppressed, but they also show a daytime maximum (Figure 7c). Fluxes at 7 m in the midnight to 08:00 period were typically of small magnitude, but the hourly means were typically positive (indicating an upward flux) and upward fluxes during this part of the day were slightly more common during the leaf-active period possibly indicating a role of the understory as a particle source.

As described above, due to concerns that during precipitation events the sonic anemometer performance may be degraded, and/or the particle measurements may be compromised by condensation in the sampling lines; a data screening criteria was applied to exclude periods when precipitation was observed from the flux ensemble data set. A separate analysis of the particle number fluxes at 46 m during precipitation events indicates a median value of $9.7 \times 10^5 \, \text{m}^{-2} \, \text{s}^{-1}$ (indicating that more than 50% of the data are associated with upward fluxes) (IQR: -4.1 to $4.8 \times 10^6 \, \text{m}^{-2} \, \text{s}^{-1}$), while comparable values during nonprecipitation hours indicate a median value of $-1.7 \times 10^6 \, \text{m}^{-2} \, \text{s}^{-1}$ (IQR: -6.5 to $5.3 \times 10^6 \, \text{m}^{-2} \, \text{s}^{-1}$). Thus, consistent with previous research [*Gordon et al.*, 2011], the flux magnitudes were generally lower and upward fluxes are more frequent during hours in which precipitation is observed. Average below canopy fluxes are also of slightly smaller magnitude during hours with precipitation than during nonprecipitation periods (median value during precipitation = $-1.1 \times 10^5 \, \text{m}^{-2} \, \text{s}^{-1}$, IQR: -1.3 to $1.5 \times 10^6 \, \text{m}^{-2} \, \text{s}^{-1}$, cf. median during nonprecipitation periods of $-1.3 \times 10^5 \, \text{m}^{-2} \, \text{s}^{-1}$, IQR: -1.7 to $1.7 \times 10^6 \, \text{m}^{-2} \, \text{s}^{-1}$).

3.1.2. Uncertainties

Best practice for computing robust flux estimates has been widely discussed within the rubric of national and global carbon flux networks [*Massman et al.*, 2003; *Moncrieff et al.*, 2004]. However, a range of different approaches have been taken to compute particle number fluxes including application of stationarity filters to exclude nonstationary periods and use of detrending. The primary argument for not using linear detrending is that it does not obey the rules of Reynolds averaging [*Moncrieff et al.*, 2004]. Nevertheless, it has been extensively used in prior studies of particle number fluxes [e.g., *Grönholm et al.*, 2009; *Pryor et al.*, 2008c], though not in all [e.g., *Gordon et al.*, 2011; *Rannik et al.*, 2009], in part because of the high probability of nonstationarity in particle concentrations. In order to investigate the importance of these methodological decisions the data set from 46 m was used to compute UFP number fluxes using three different procedures: (a) one in which the raw concentration time series were only despiked but otherwise were used "as is" (the base case), (b) one in which the concentration time series were also subject to linear detrending, and (c) one in which the time series from (a) were subject to a stationarity test [*Foken and Wichura*, 1996]. In this stationarity analysis each 24 min time series was evenly divided into six subsets. If the mean of the variance of the subsets deviates by less than 30% from the variance of full time series, it is considered stationary. This test for stationarity is failed for over half of the EC derived fluxes above the canopy; however, exclusion of those cases does not change the partitioning of the flux between upward and downward cases. This result implies that the upward fluxes are not solely a result of nonstationarity in the time series of UFP number concentrations. The impact of linear detrending is large. The conditional probability that the flux from the detrended time series indicates an upward flux under the condition that F from the "raw" time series is also positive is 70%, while conditional probability of the flux estimates from (a) and (b) being downward is 74%. Fluxes derived from the detrended and raw time series were fitted to a linear model using multiple least squares regression (where y is the flux from the detrended time series and x is the flux from the raw time series). The parameters of this fit indicate a slope of 0.95 and an adjusted r^2 of 0.73. When only cases where $F > \delta F$ are considered the parameters of a linear fit between F from the raw series and those that have been detrended indicate a slope of 0.95 and an adjusted r^2 of 0.74. Thus, exclusion of periods with high relative flux uncertainty only slightly improves the agreement between flux estimates derived with and without linear detrending, and use of linear detrending alters both the magnitude of the fluxes and the sign (direction) of a substantial fraction of the flux estimates. This finding implies that great care should be taken when comparing UFP number flux estimates from different studies conducted over different forest types using different flux methodologies and assumptions. The UFP number fluxes computed for MMSF without detrending are used in all following analyses.

3.1.3. Importance of the Storage Flux

Fluxes derived using eddy covariance explicitly describe the vertical flux of particles through some reference level above the surface; however, other processes can alter the actual atmosphere-surface exchange. Key among these is the storage flux [*Gordon et al.*, 2011; *Rannik et al.*, 2009]. F_{store} computed from the UFP data collected at 46 m is frequently of a similar magnitude to F as estimated by using EC (Figure 8a). Although the absolute value of the ratio F_{store}/F is generally below 1 (85% of all periods), it is above 0.5 for 41% of all periods. This implies that F_{store} is a significant component of the UFP budget and substantially alters the actual surface uptake relative to that implied by EC conducted at 18 m above the canopy. Consistent with the a priori expectation that F_{store} will be of largest relative magnitude when turbulence is weak and/or during the early morning, 80% of F_{store}/F ratios are below 1 when all turbulence conditions (including $u_* < 0.2 \, \mathrm{m \, s^{-1}}$) are considered. Although the relative importance of the storage flux in the conservation equation for particle number concentrations at MMSF is smaller than that computed for the SMEAR II measurement station where 31% of periods had a F_{store}/F ratio of >1 [*Rannik et al.*, 2009], this term is far from negligible. No clear diurnal cycle was found in F_{store}/F, but values were typically largest in the nighttime hours and smallest in the middle of the day consistent with the diurnal variability in the vertical flux.

3.1.4. Fluxes During Nucleation Episodes

It has previously been postulated that during the early morning hours as the boundary layer grows, "clean" (low particle concentration) air may be entrained from above the nocturnal inversion, potentially leading both to upward fluxes of particle number and conditions conducive to new particle formation [*Nilsson et al.*, 2001; *Pryor et al.*, 2008a]. Particle nucleation in turn causes a rapid increase in the number concentration of UFP and associated changes in F_{store} and F. Data from MMSF exhibit some consistency with this qualitative
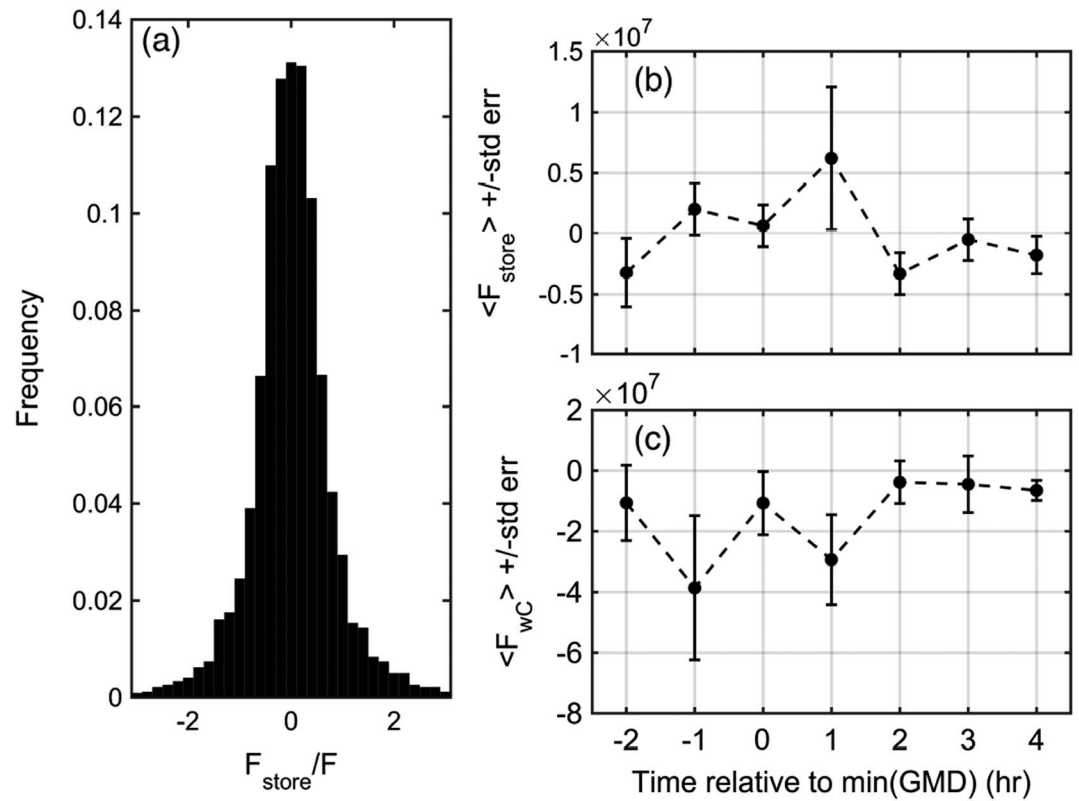
Figure 8. (a) Histogram of the ratio of the Storage flux to the EC derived flux (F_{store}/F) at 46 m. Mean and standard error (std err $= \sigma/\sqrt{n}$) of (b) the particle storage flux (F_{store}, in # m^{-2} s^{-1}) and (c) the UFP number flux at 46 m determined by using eddy covariance (F_{wC}, in # m^{-2} s^{-1}) during nucleation events. In frames in Figures 8b and 8c the x axis has been normalized such that 0 is the time at which the minimum geometric mean diameter (min(GMD)) was observed for each of the nucleation cases in the particle size distribution measurements at 28 m.

expectation of the impact of these events on both the flux and storage term, although the event-to-event variability is large. When the flux data are conditionally sampled by the occurrence of A-class particle nucleation events, the mean F_{store} (± 1 standard error) is negative 2 h prior to the min(GMD) consistent with particle nucleation being preceded by entrainment of clean air from above the inversion leading to negative F_{store}. During this hour the mean flux is negative but the associated standard error crosses the zero point, indicating a substantial portion of the fluxes are upward 2 h prior to the occurrence of min(GMD) (Figures 8b and 8c). During the nucleation event (1 h prior to min(GMD) to 1 h after min(GMD)) as new particles are being formed F_{store} is positive and F is downward and of large magnitude. At the peak of the NPF event (hour = 0) the vertical flux is comparatively small and F_{store} decreases possibly due to ventilation of UFP from the canopy. Beyond 2 h after min(GMD) mean F_{store} is small and negative and mean F is also negative (Figures 8b and 8c).

3.1.5. Diagnosing Upward Fluxes

As described above, a substantial fraction of UFP number fluxes above (and below) the canopy are upward. To investigate the causes of this phenomenon, the scalar correlation coefficients (R_{xy}) between sonic virtual temperature, water vapor, vertical velocity, and particle number concentrations were investigated during the upper 25% of UFP number fluxes during the time for which the LiCOR LI-7200 data were available. The occurrence of these large-magnitude upward fluxes is restricted almost exclusively to the daylight days (almost exclusively between 09:00 and 18:00 LST) with a peak in the early afternoon (approximately 13:00 LST) and a secondary peak in the late morning (around 11:00 LST) (Figure 9a). Thus, there is an expectation that these events may include contributions both from entrainment (largely during the morning) and venting of UFP grown to detectable size within the canopy (afternoon). The results show qualitative agreement with this expectation. The probability distribution of R_{wT} is quasi-bimodal with a mode centered on values ≈ -0.4 and a second mode centered at ≈ 0.5 (Figure 9b). Conceptually, the first is linked to entrainment of warm air from above the nocturnal inversion, while the latter might reasonably be ascribed to fluxes during the
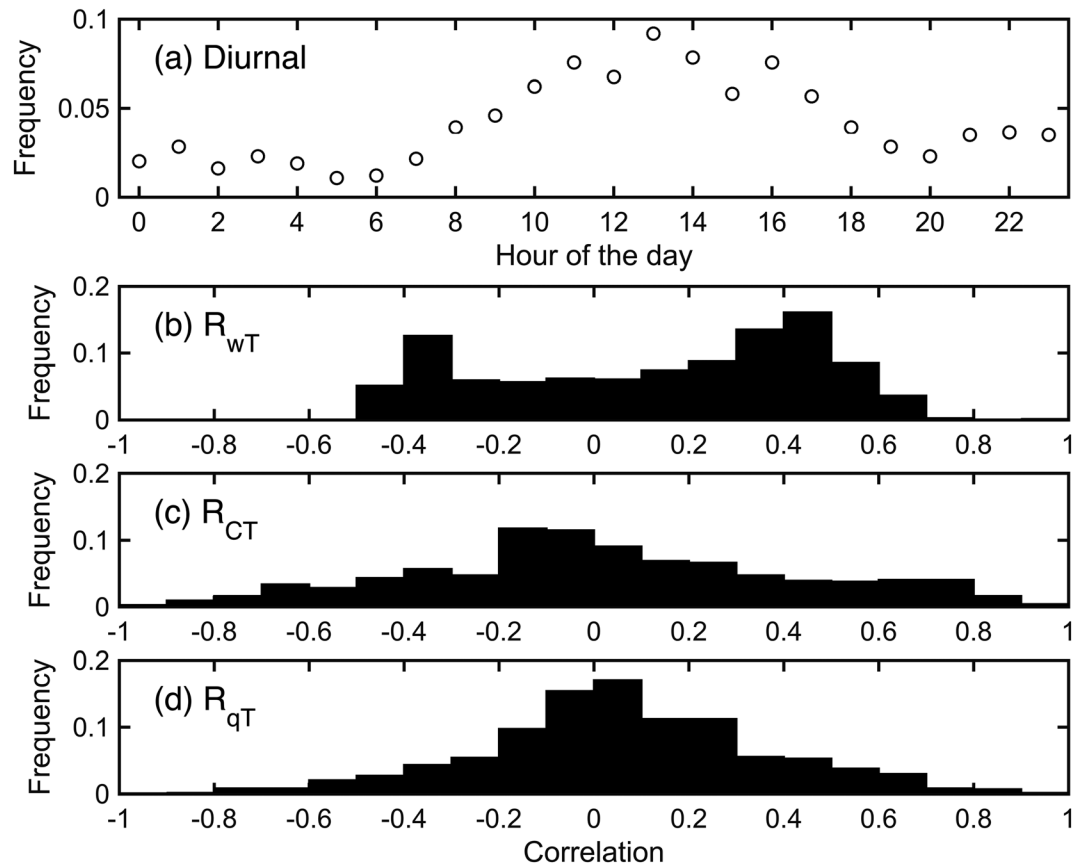
Figure 9. (a) Diurnal profile of the frequency with which the highest 25% of particle number fluxes (i.e., the strongest apparent upward fluxes) are observed. Also shown are correlation coefficients (R_{xy}) computed from 10 Hz data from the 46 m sampling level during these cases. The correlations are shown between (b) sonic virtual temperature (T) and vertical velocity (w), (c) UFP number concentrations (C) and sonic virtual temperature (T), and (d) sonic virtual temperature (T) and the water vapor concentration (q) from the LiCOR LI-7200.

afternoon during convective conditions. R_{CT} span a very wide range of values but are biased toward positive values (consistent with daytime results obtained over an orchard [*Held et al.*, 2008]). Values of R_{qT} are almost equally distributed between positive and negative values (Figure 9d). This analysis of scalar correlation coefficients is consistent with, but not proof of, the occurrence of two phenomena; entrainment from above the inversion and venting of particles from the canopy. The large number of hours in which both R_{CT} and R_{qT} are effectively "decoupled" (i.e., low correlation values; Figures 9c and 9d) may reflect a bias toward sampling of near-neutral conditions (by conditional sampling for $u_* > 0.2$) but may also link to particle dynamics. For example, the decoupling of C and T may occur due to coagulation of particles (which would cause variability in C not associated with variation in T), while low values of R_{qT} may be symptomatic of partitioning of water onto the particle surface during transport.

3.2. Flux Partitioning Between the Canopy and Ground

The preceding discussion implies that great caution should be taken in inferring surface exchange (e.g., deposition velocities) from the flux. Nevertheless, an attempt was made to use the data from the two-level system to provide a first estimate of the canopy versus below-canopy uptake.

The flux ratio (FR = F_7/F_{46}) and interception fraction (I) from MMSF lie within the range of estimates available in the literature for particle fluxes to forests based on accumulation measurements (0.6–0.9) (as summarized in *Grönholm et al.* [2009]), and when conditionally sampled by canopy status exhibit the expected behavior of increased I during the leaf-active period, and decreased canopy uptake during the leaf-off period (Table 1). Median-I for the entire data set = 0.73, during the leaf-active period it is 0.78, and during the leaf-off period it is 0.70. However, the interquartile range (IQR) on all estimates is large indicating substantial day-to-day

Table 1. Summary Statistics of the Flux Ratio (FR) Computed From the Particle Number Fluxes Above (F_{46}) and Below (F_7) the Canopy During Deposition Periods When $u_* > 0.2 \, \text{m s}^{-1}$, and the Derived Estimates of Canopy Interception Fraction (I, From Equation (7))

	All Periods	Leaf-Active	Leaf-Off
Median (and mean) flux ratio: F_7/F_{46}	0.22 (0.32)	0.19 (0.31)	0.24 (0.33)
Median (and interquartile range) of I	0.73 (0.55–0.83)	0.78 (0.58–0.86)	0.70 (0.53–0.81)

variability (Table 1). Median-I computed for the data set collected at the MMSF deciduous forest thus exceeds the value reported for the SMEAR-II pine forest (of 0.62), despite laboratory studies that have generally indicated higher deposition velocities to needleleaf trees were higher than to broadleaf trees [*Hwang et al.*, 2011]. This may reflect the higher double-sided *LAI* of MMSF, or differences in the turbulence regimes at the two sites (MMSF v. SMEAR II), use of a u_* threshold herein, or the different cut-points of the two CPCs used in the SMEAR II and MMSF campaigns given that deposition velocities of sub-30 nm diameter particles to forest canopies tend to increase rapidly with decreasing D_p [*Pryor et al.*, 2009]. Thus, the lower cut-point of the CPC used at MMSF may be partially responsible for the higher canopy uptake computed for the current study. Data collected at MMSF for the leaf-active period indicate that the median FR declines with increasing u_*, from ~0.26 at a $u_* \sim 0.25 \, \text{m s}^{-1}$ to ~0.15 at $u_* > 1.0 \, \text{m s}^{-1}$ and a linear fit to this relationship has a slope of -0.06, though the adjusted r^2 value is only 0.21, indicating substantial scatter in the data and/or a nonlinear relationship. Similar results for the SMEAR-II forest indicate FR ~ 0.35 for $u_* = 0.20$–$0.25 \, \text{m s}^{-1}$ declining to 0.10 for $u_* > 1.0 \, \text{m s}^{-1}$. Thus, the inference from these analyses is that the deciduous canopy at MMSF on average captures a large fraction of the deposited UFP and that even during leaf-off the deciduous canopy captures the majority of the UFP. This latter finding might reflect the large amount of woody material in the canopy of this mature forest (see canopy photographs in Figure 1) and that even during the leaf-off period the mean-LAI at MMSF is $1.2 \, \text{m}^2 \, \text{m}^{-2}$, or the importance of the leaf-area distribution in determining the UFP flux to the canopy [*Huang et al.*, 2013].

No differentiable impact of stomata penetration on the UFP flux to the canopy could be found by comparing FR during deposition periods within the leaf-active dates during daytime and nighttime. The median FR during the daytime (i.e., 10:00–16:00, inclusive) was 0.18 (IQR: 0.10–0.33), while that during the nighttime (i.e., 22:00–04:00, inclusive) was 0.19 (IQR: 0.12–0.38). Thus, other factors (e.g., differences in u_*) mask any impact of stomata penetration on canopy capture of UFP.

4. Instrumentation Discussion

Making robust flux measurements of UFP and interpreting them correctly remains extremely challenging. The study presented herein was uniquely ambitious regarding the duration of sampling attempted with the two-layer measurement system. Our experience highlights two key challenges that are not unique to our analysis and merit further discussion:

1. Particle instruments remain relatively bulky; thus, it is impractical to deploy them on a meteorological support structure designed for high-quality flux measurements in which minimization of flow distortions is of great importance. Further, the operation of most particle instruments remains highly sensitive to temperature fluctuations. Many forests in midlatitude regions (such as southern Indiana) experience a wide range of hourly mean temperature (for the current study period the range was -20 to 48°C), while many CPCs have an operating range of 10–30°C. For these reasons, in our study we chose to deploy the CPC in a temperature-controlled instrument hut, which thus required long sampling lines that result in dampening of the high frequencies. This, in conjunction with the lack of true 10 Hz response in the CPC (evident in Figure 5, and discussed previously elsewhere [e.g., *Held et al.*, 2008]), present real challenges to use of eddy covariance.

2. Many instruments designed to measure UFP use a working fluid (water or isobutanol for most) to swell the particles for detection. They thus have complex fluid (gas and liquid) flows that have to be carefully controlled to avoid flooding of the optics. Because the intent of this study was to compare UFP number fluxes above and below the canopy a decision was made to use a single CPC and employ a switching mechanism. This meant that the CPCs were subject to repeated faults related in part to the pressure drop across the instrument during valve switching between sampling lines and also a number of issues related

to flow control within the instrument. The switching also meant that the sampling duration over which fluxes could be calculated is likely suboptimal particularly given evidence that a longer integration period for flux calculation may be necessary for particle number fluxes than for other scalars [*Pryor et al.*, 2008b].

There remain major questions regarding vertical flux divergence for aerosol particles. Differentiating these effects and correctly quantifying the associated uncertainties based solely on experimental data remains very challenging particularly given these measurement issues. Thus, there is a real need for continued development of new instruments in order to particle flux measurements to reach the standards of accuracy and reliability required for model validation and verification exercises.

5. Concluding Remarks

There is a continued need to improve understanding of atmosphere-surface exchange of UFP. This study sought to develop a climatologically representative and relevant flux data set for UFP exchange over and in a deciduous forest, and despite technical challenges, the results from over 4000 h of data representative of both leaf-active and leaf-off conditions suggest the following:

1. Despite the occurrence of a large number of upward fluxes of UFP (46% of the time) on average the forest is a net sink for UFP. This is true both during leaf-active and leaf-off periods, and the overall mean above-canopy flux conditionally sampled for $u_* > 0.2\,\mathrm{m\,s^{-1}}$ is $-4.9 \times 10^6\,\mathrm{m^{-2}\,s^{-1}}$. Assuming this is a representative value, it implies an annual total removal of UFP of almost $3.2 \times 10^{14}\,\mathrm{m^{-2}}$. While this estimate must be viewed with great caution and is applicable only to this forest in this (highly-polluted) environment, it re-emphasizes the potential importance of forests to UFP removal and the need to improve such estimates.
2. UFP flux estimates are subject to relatively large uncertainty due in part to our inability to fully capture the range of scales that contribute to the transfer with currently available particle counting instrumentation. Nonetheless, very good agreement was obtained between fluxes calculated from the EC and REA processing. However, there is an urgent need for continued advancement of new measurement technologies.
3. Treatment of the data time series, in particular detrending, has a major impact on the flux results, which leads to great challenges in comparing flux estimates from different studies.
4. The storage flux is a large contributor to the budget of UFP over forests and greatly confounds translation of EC fluxes to true surface exchange.
5. Despite the large uncertainties, above the canopy the mean flux is shown to be downward throughout the day (except at 23.00) with the magnitude of the flux being larger during the middle of the day. Separating the impact of transport/meteorological processes from aerosol dynamics remains highly challenging, particularly since humidity and CO_2 fluxes are also subject to the impact of nonmeteorological phenomena.
6. The caveats implied by the above naturally means that caution should be applied in assessing the results for the flux partitioning between the canopy and the ground. However, first-order estimates derived herein implies that 73% (55–83%) of the UFP capture by the ecosystem occurs at the canopy of the over-storey. This fraction increases to 78% during the leaf-active period but is also 70% during the leaf-off period.

References

Aubinet, M., J. Moncrieff, and R. C. Clement (2000), Estimates of the annual net carbon and water exchange of forests: The EUROFLUX methodology, *Adv. Ecol. Res.*, *30*, 113–175.

Boucher, O., D. Randall, P. Artaxo, C. Bretherton, G. Feingold, P. Forster, V.-M. Kerminen, Y. Kondo, H. Liao, and U. Lohmann (2013), Clouds and aerosols, in *Climate Change 2013: The Physical Science Basis. Contribution of Working Group I to the Fifth Assessment Report of the Intergovernmental Panel on Climate Change*, edited, pp. 571–657, Cambridge Univ. Press, Cambridge, New York.

Burkhardt, J. (2010), Hygroscopic particles on leaves: nutrients or desiccants?, *Ecol. Monogr.*, *80*(3), 369–399.

Businger, J. A., and S. P. Oncley (1990), Flux measurement with conditional sampling, *J. Atmos. Oceanic Technol.*, *7*, 349–352.

Buzorius, G., Ü. Rannik, D. Nilsson, and M. Kulmala (2001), Vertical fluxes and micrometeorology during aerosol particle formation events, *Tellus*, *53B*, 394–495.

Dadvand, P., I. Rivas, X. Basagaña, M. Alvarez-Pedrerol, J. Su, M. D. C. Pascual, F. Amato, M. Jerret, X. Querol, and J. Sunyer (2015), The association between greenness and traffic-related air pollution at schools, *Sci. Total Environ.*, *523*, 59–63.

Dal Maso, M., M. Kulmala, I. Riipinen, R. Wagner, T. Hussein, P. P. Aalto, and K. E. J. Lehtinen (2005), Formation and growth of fresh atmospheric aerosols: Eight years of aerosol size distribution data from SMEAR II, Hyytiala, Finland, *Boreal Environ. Res.*, *10*(5), 323–336.

Eugster, W., and W. Senn (1995), A cospectral correction model for measurement of turbulent NO2 flux, *Bound.-Lay. Meteorol.*, *74*(4), 321–340.

Finnigan, J. (2000), Turbulence in plant canopies, *Annu. Rev. Fluid Mech.*, *32*, 519–571.

Foken, T., and B. Wichura (1996), Tools for quality assessment of surface-based flux measurements, *Agr. Forest Meteorol.*, *78*, 83–105.

Froelich, N. J., C. S. B. Grimmond, and H. P. Schmid (2011), Nocturnal cooling below a forest canopy: Model and evaluation, *Agr. Forest Meteorol.*, *151*(7), 957–968, doi:10.1016/j.agrformet.2011.02.015.

Gordon, M., R. Staebler, J. Liggio, A. Vlasenko, S.-M. Li, and K. Hayden (2011), Aerosol flux measurements above a mixed forest at Borden, Ontario, *Atmos. Chem. Phys.*, *11*(14), 6773–6786.

Grönholm, T., S. Launiainen, L. Ahlm, E. M. Martensson, M. Kulmala, T. Vesala, and E. D. Nilsson (2009), Aerosol particle dry deposition to canopy and forest floor measured by two-layer eddy covariance system, *J. Geophys. Res.*, *114*, D04202, doi:10.1029/2008JD010663.

Held, A., E. Patton, L. Rizzo, J. Smith, A. Turnipseed, and A. Guenther (2008), Relaxed eddy accumulation simulations of aerosol number fluxes and potential proxy scalars, *Bound.-Lay. Meteorol.*, *129*(3), 451–468, doi:10.1007/s10546-008-9327-5.

Hosker, R. P., and S. Lindberg (1982), Review: Atmospheric deposition and plant assimilation of gases and particles, *Atmos. Environ.*, *16*, 889–910.

Huang, C.-W., M.-Y. Lin, A. Khlystov, and G. Katul (2013), The effects of leaf area density variation on the particle collection efficiency in the size range of ultrafine particles (UFP), *Environ. Sci. Technol.*, *47*(20), 11,607–11,615.

Hwang, H.-J., S.-J. Yook, and K.-H. Ahn (2011), Experimental investigation of submicron and ultrafine soot particle removal by tree leaves, *Atmos. Environ.*, *45*(38), 6987–6994.

Kaimal, J. C., and J. J. Finnigan (1994), *Atmospheric Boundary Layer Flows: Their Structure and Measurement*, 289 pp., Oxford Univ. Press, New York.

Katul, G. G., P. L. Finkelstein, J. F. Clarke, and T. G. Ellestad (1996), An investigation of the conditional sampling method used to estimate fluxes of active, reactive, and passive scalars, *J. Appl. Meteorol.*, *35*(10), 1835–1845.

Kowalski, A. (2001), Deliquescence induces eddy covariance and estimable dry deposition errors, *Atmos. Environ.*, *35*, 4843–4851.

Kumar, P., A. Wiedensohler, W. Birmili, P. Quincey, and M. Hallquist (2016), Ultrafine particle pollution and measurements, *Compr. Anal. Chem.*, *73*, 369–390.

Kupc, A., O. Bischof, T. Tritscher, M. Beeston, T. Krinke, and P. E. Wagner (2013), Laboratory characterization of a new nano-water-based CPC 3788 and performance comparison to an ultrafine butanol-based CPC 3776, *Aerosol Sci. Technol.*, *47*(2), 183–191.

Massman, W., J. Finnigan, D. Billesbach, S. Miller, A. Black, B. Amiro, B. Law, X. Lee, L. Mahrt, and R. Dahlman (2003), Summary and synthesis of recommendations of the AmeriFlux Workshop on standardization of flux analysis and diagnostics, AmeriFlux Network, AmeriFlux Workshop Team, Oak Ridge Natl. Lab., Oak Ridge, Tenn. [Available from: http://public.ornl.gov/ameriflux/workshops/workshop-20020827-corvallisOR-summary.doc, Corvallis, Oregon; August 2002.]

Moncrieff, J., R. Clement, J. Finnigan, and T. Meyers (2004), Averaging, detrending, and filtering of eddy covariance time series, in *Handbook of Micrometeorology*, edited by X. Lee, W. J. Massman, and B. E. Law, pp. 7–31, Kluwer Acad., Dordrecht, Netherlands.

Nilsson, E. D., Ü. Rannik, M. Kulmala, G. Buzorius, and C. O'Dowd (2001), Effects of continental boundary layer evolution, convection, turbulence and entrainment, on aerosol formation, *Tellus*, *53B*, 441–461.

Ould-Dada, Z. (2002), Dry deposition profile of small particle within a model spruce canopy, *Sci. Total Environ.*, *286*, 83–96.

Pataki, D. E., M. M. Carreiro, J. Cherrier, N. E. Grulke, V. Jennings, S. Pincetl, R. V. Pouyat, T. H. Whitlow, and W. C. Zipperer (2011), Coupling biogeochemical cycles in urban environments: Ecosystem services, green solutions, and misconceptions, *Front. Ecol. Environ.*, *9*(1), 27–36.

Petroff, A., A. Mailliat, M. Amielh, and F. Anselmet (2008), Aerosol dry deposition on vegetative canopies. Part II: A new modelling approach and applications, *Atmos. Environ.*, *42*(16), 3654–3683, doi:10.1016/j.atmosenv.2007.12.060.

Pryor, S. C., and F. S. Binkowski (2004), An analysis of the time scales associated with aerosol processes during dry deposition, *Aerosol Sci. Technol.*, *38*, 1091–1098.

Pryor, S. C., R. J. Barthelmie, S. E. Larsen, L. L. Sørensen, A. M. Sempreviva, T. Grönholm, M. Kulmala, Ú. Rannik, and T. Vesala (2008a), Upward particle number fluxes over forest: Where, when, why?, *Tellus*, *60B*, 372–380.

Pryor, S. C., et al. (2008b), A review of measurement and modelling results of particle atmosphere-surface exchange, *Tellus B*, *60*, 42–75.

Pryor, S. C., S. E. Larsen, L. L. Sørensen, and R. J. Barthelmie (2008c), Particle fluxes above forests: Observations, methodological considerations and method comparisons, *Environ. Pollut.*, *152*(3), 667–678.

Pryor, S. C., R. J. Barthelmie, A. M. Spaulding, S. E. Larsen, and A. Petroff (2009), Size-resolved aerosol particle fluxes over forests, *J. Geophys. Res.*, *114*, D18212, doi:10.1029/2009JD012248.

Pryor, S. C., A. M. Spaulding, and R. J. Barthelmie (2010), New particle formation in the Midwestern USA: Event characteristics, meteorological context and vertical profiles, *Atmos. Environ.*, *44*, 4413–4425.

Pryor, S. C., R. J. Barthelmie, and K. E. Hornsby (2013), Size-resolved particle fluxes and vertical gradients over and in a sparse pine forest, *Aerosol Sci. Technol.*, *47*(11), 1248–1257.

Pryor, S. C., K. E. Hornsby, and K. A. Novick (2014), Forest canopy interactions with nucleation mode particles, *Atmos. Chem. Phys.*, *14*(21), 11,985–11,996, doi:10.5194/acp-14-11985-2014.

Rannik, Ü., P. Aalto, P. Keronen, T. Vesala, and M. Kulmala (2003), Interpretation of aerosol particle fluxes over a pine forest: Dry deposition and random errors, *J. Geophys. Res.*, *108*(D17), 4544, doi:10.1029/2003JD003542.

Rannik, Ü., I. Mammarella, P. Aalto, P. Keronen, T. Vesala, and M. Kulmala (2009), Long-term aerosol particle flux observations. Part I: Uncertainties and time-average statistics, *Atmos. Environ.*, *43*(21), 3431–3439.

Rannik, Ü., L. Zhou, P. Zhou, R. Gierens, I. Mammarella, A. Sogachev, and M. Boy (2016), Aerosol dynamics within and above forest in relation to turbulent transport and dry deposition, *Atmos. Chem. Phys.*, *16*(5), 3145–3160.

Roman, D., K. Novick, E. Brzostek, D. Dragoni, F. Rahman, and R. Phillips (2015), The role of isohydric and anisohydric species in determining ecosystem-scale response to severe drought, *Oecologia*, *179*(3), 641–654.

Schmid, H. P., C. S. B. Grimmond, F. Cropley, B. Offerle, and H.-B. Su (2000), Measurements of CO2 and energy fluxes over a mixed hardwood forest in the midwestern United States, *Agr. Forest Meteorol.*, *103*, 357–374.

Su, H.-B., H. P. Schmid, C. S. B. Grimmond, C. S. Vogel, and A. J. Oliphant (2004), Spectral characteristics and correction of long-term eddy-covariance measurements over two mixed hardwood forests in non-flat terrain, *Bound.-Lay. Meteorol.*, *110*(2), 213–253, doi:10.1023/a:1026099523505.

Sullivan, R. C., and S. C. Pryor (2016), Dynamic and chemical controls on new particle formation occurrence and characteristics from in situ and satellite-based measurements, *Atmos. Environ.*, *127*, 316–325.

Teklemariam, T., R. Staebler, and A. Barr (2009), Eight years of carbon dioxide exchange above a mixed forest at Borden, Ontario, *Agr. Forest Meteorol.*, *149*(11), 2040–2053.

Webb, E., G. Pearman, and R. Leuning (1980), Correction of flux measurements for density effects due to heat and water vapour transfer, *Q. J. R. Meteorol. Soc.*, *106*, 85–100.

Wyngaard, J. C. (1973), On surface-layer turbulence, in *Workshop on Micrometeorology*, edited by D. A. Haugen, pp. 101–149, Am. Meteorol. Soc., Boston, Mass.

Wyngaard, J. C., and C.-H. Moeng (1992), Parameterizing turbulent diffusion through the joint probability density, *Bound.-Lay. Meteorol.*, *60*(1-2), 1–13.